Current Controller Based on Reduced Order Generalized Integrators for Distributed Generation Systems

Claudio Alberto Busada, Sebastián Gómez Jorge, Andres E. Leon, *Graduate Student Member, IEEE*, and Jorge A. Solsona, *Senior Member, IEEE*

***Abstract*—This paper presents a current controller based on a stationary reference frame implementation of an integrator in the synchronous reference frame [called here reduced order generalized integrator (ROGI)], suitable for three-phase distributed generation systems. The proposed controller is compared with the traditional second-order generalized integrator (SOGI)-based current controller. It is confirmed that, in normal operation conditions, both controllers have similar performance, requiring the ROGI-based controller much less computational burden than the SOGI counterpart. The proposed controller injects sinusoidal currents synchronized with the grid voltage, without requiring any dedicated synchronization algorithm. Three different current injection strategies are realizable with the same controller structure: balanced current injection, constant instantaneous active power injection, and maximum instantaneous active power injection. A state-variable-based control methodology in the discrete-time domain is presented. It ensures the stability and performance of the closed-loop system, even for high-order controllers and large digital signal processor processing delay. Moreover, it is confirmed that the proposed controller works satisfactorily even on faulty grid conditions.**

***Index Terms*—Current controller, distributed generation, generalized integrator, resonant controller, second-order generalized integrator (SOGI), voltage source converter (VSC).**

I. Introduction

A COMMON element in distributed power generation systems (DPGSs), whatever the primary energy source is (fuel cells, solar panels, or wind turbines), is a voltage source converter (VSC), which is usually connected to the distribution network as shown in Fig. 1 [1]–[5]. The converter should fulfill the following characteristics regarding current injection:

1) ensuring high-quality injected currents;
2) proper synchronization with the network;
3) satisfactory performance of the system when faced with a network failure scenario.

Manuscript received February 22, 2011; revised July 4, 2011; accepted August 15, 2011. Date of publication September 15, 2011; date of current version February 17, 2012. This work was supported in part by Universidad Nacional del Sur, by Consejo Nacional de Investigaciones Científicas y Técnicas (CONICET), and by Agencia Nacional de Promoción Científica y Tecnológica (ANPCyT), Argentina.

The authors are with the Instituto de Investigaciones en Ingeniería Eléctrica "Alfredo Desages" [Universidad Nacional del Sur (UNS)–Consejo Nacional de Investigaciones Científicas y Técnicas (CONICET)], Departamento de Ingeniería Eléctrica y de Computadoras, UNS, Bahía Blanca 8000, Argentina (e-mail: cbusada@uns.edu.ar; sebastian.gomezjorge@uns.edu.ar; aleon@ymail.com; jsolsona@uns.edu.ar).

Digital Object Identifier 10.1109/TIE.2011.2167892

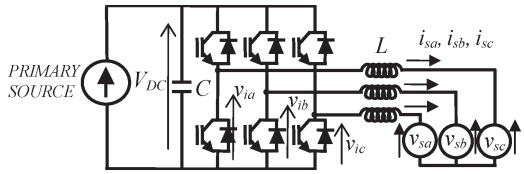

Fig. 1. Grid-connected VSC.

Regarding 1), DPGSs are considered generators themselves, and they are subject, as power quality concerns, to quality standards more stringent than consumers. For example, IEEE Standard 1547-2003 [6] recommends a total harmonic distortion factor (THD) of less than 5%. The quality of the injected current is defined by the current control strategy used. The most popular current controllers in DPGS are hysteresis controllers, predictive controllers, and proportional–integral (PI)-type linear controllers [7]–[11]. In digital implementation, the last two are preferred. A PI current controller implemented in the stationary reference frame nullifies the error between the controlled variable and reference variable if these signals have their frequency content where the controller has infinite gain, that is, at zero frequency. When such PI acts on signals that have the grid frequency (ω_0), both amplitude and phase errors occur. To eliminate these errors, the PI is typically implemented in a synchronous reference frame [12] rotating at $(+\omega_0)$, where ac signals appear as dc signals. This assures, in harmonic-free balanced systems, zero tracking error between the injected currents and their references. In unbalanced systems, a second PI implemented in a reference frame rotating in the opposite direction $(-\omega_0)$ is usually included in the current controller [13]. In systems containing voltage harmonics, several PIs, implemented each in a reference frame rotating with the frequency of their associated harmonic, are included [14]. PI controllers implemented in rotating reference frames require transforming the signals from the stationary reference frame to the synchronous reference frame and antitransform the resulting control actions. This implies an additional computational burden. In [15], a synchronous current controller implemented in a stationary reference frame is presented. This eliminates the need to transform and antitransform the signals, still obtaining a controller with infinite gain at fundamental grid frequency. In [16]–[18], second-order generalized integrators (SOGIs) are used to synthesize resonant current controllers implemented in the stationary reference frame, which have infinite gain at the fundamental frequency, and produce a similar result. Incorporating multiple SOGIs, these resonant systems can be used

in controllers that operate in networks containing harmonics and imbalance [19], [20]. In [21]–[23], in order to reduce the number of states of the controller, SOGI-based resonant controllers are implemented in a synchronous reference frame rotating at the fundamental frequency.

Regarding 2), the reference currents that the controller will track must be high-quality sinusoidal signals, properly synchronized with the grid voltages. To synthesize these signals, different algorithms have been developed. These are responsible for extracting the angle of the grid voltage fundamental component, and using this, to synthesize the required current references. The most popular algorithms are those based on the phase-locked loop technique, frequency-locked loop technique, and filtering of grid voltage [24]–[27]. In order to separate positive and negative sequence components, a delayed signal cancellation method is also implemented in [28] and [29], and a signal model-based observer is proposed in [30] and [31]. Additionally, algorithms based on either discrete Fourier transform or Kalman filter can be found [32], [33]. Synchronization algorithms must operate correctly even under severe voltage unbalance conditions (SVUC) and in the presence of voltage harmonics.

Regarding 3), the DPGS controller must ensure, for a short stipulated period of time, the satisfactory performance during a fault (for example, the short circuit between two phases or between one or two phases and neutral). In these fault cases, the network suffers a severe voltage unbalance, which must be withstood successfully by the DPGS. Several techniques have been proposed to generate the current reference to be followed during a failure scenario. They basically require to extract the positive and negative sequence fundamental components of voltages and currents, a task that imposes a high computational burden [34]–[36].

In this paper, a current controller based on the stationary reference frame implementation of a synchronous integrator [(herein called reduced order generalized integrator (ROGI)] is proposed. This controller fulfills the three mentioned requirements with a very low processing load compared with related proposals. The original elements of the proposed controller with respect to previous works are as follows.

1) It synthesizes harmonic-free currents that are properly synchronized, without requiring any dedicated synchronization algorithm to synchronize or synthesize current references.
2) It allows, by changing a single parameter, to select (online) between three different strategies commonly used to cope with failure scenarios [34].
3) It has a significantly lighter computational burden than similar proposals, achieving virtually the same performance than its counterparts.

The controller design is performed in the stationary reference frame, not requiring any variable reference frame change. A digital domain controller design methodology is also presented. It ensures a systematic and robust design of high-order controllers, even in the presence of large digital signal processor (DSP) processing delays. The proposal is validated by the frequency response method, simulations, and experimental results.

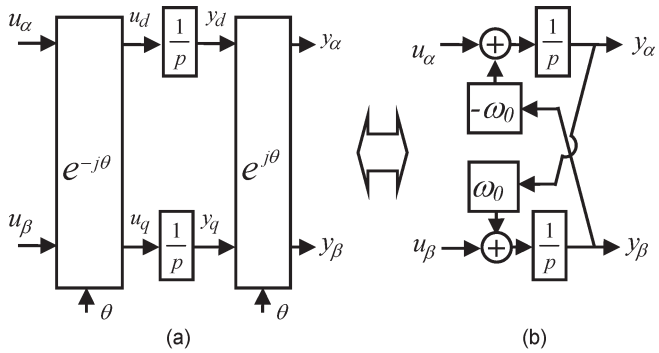

Fig. 2. Synchronous integrator. (a) dq reference frame. (b) $\alpha\beta$ reference frame.

II. ROGI

In what follows, complex space vector notation will be used. With this approach, the differential equations will have complex coefficients, where multiplying by imaginary gains implies the cross coupling between the $\alpha\beta$ axis. In complex space vector notation, transfer functions have complex coefficients, poles do not necessarily appear in conjugate pairs, and frequency responses are not necessarily symmetrical about zero [37]–[39]. An integrator, implemented in a dq reference frame that is rotated an angle θ with respect to the stationary $\alpha\beta$ reference frame, with input $\vec{u}^{dq} = u_d + ju_q$ and output $\vec{y}^{dq} = y_d + jy_q$ (see Fig. 2(a)), is described by

$$p\vec{y}^{dq} = \vec{u}^{dq} \tag{1}$$

where p is the derivative operator. This integrator is known as synchronous integrator. The relation between the variables in the dq reference frame and the variables in the $\alpha\beta$ reference frame is $\vec{u}^{dq} = e^{-j\theta}\vec{u}^{\alpha\beta}$, $\vec{y}^{dq} = e^{-j\theta}\vec{y}^{\alpha\beta}$. By applying this variable change to (1), it becomes

$$\vec{y}^{\alpha\beta} = \frac{\vec{u}^{\alpha\beta}}{p - j\omega_0} \tag{2}$$

where $\omega_0 = p\theta$. Equation (2) is the representation in the $\alpha\beta$ reference frame of (1). This representation is illustrated in Fig. 2(b). For reasons that will be explained in the following, we name (2) as ROGI. In [15], this representation is used to implement a synchronous PI in the $\alpha\beta$ reference frame.

In order to obtain the frequency response of (2), an input vector $\vec{u}^{\alpha\beta} = e^{j\omega t}$ must be applied, and the steady-state output ($\vec{y}^{\alpha\beta} = Ye^{j(\omega t+\psi)}$) must be evaluated. With such an input, at steady state, it holds that $p\vec{y}^{\alpha\beta} = j\omega\vec{y}^{\alpha\beta}$. Using this fact in (2), the following can be found:

$$Ye^{j\psi} = \frac{1}{j(\omega - \omega_0)}. \tag{3}$$

The resulting frequency response (magnitude) is shown in Fig. 3(a), for $\omega_0 = 2\pi 50$ rad/s. The response to positive frequencies is the response to a positive sequence input vector $\vec{u}^{\alpha\beta}$, and the response to negative frequencies is the response to a negative sequence input vector. Note that the ROGI system provides infinite gain to a positive sequence input vector of frequency ω_0 and attenuates negative sequence vectors.

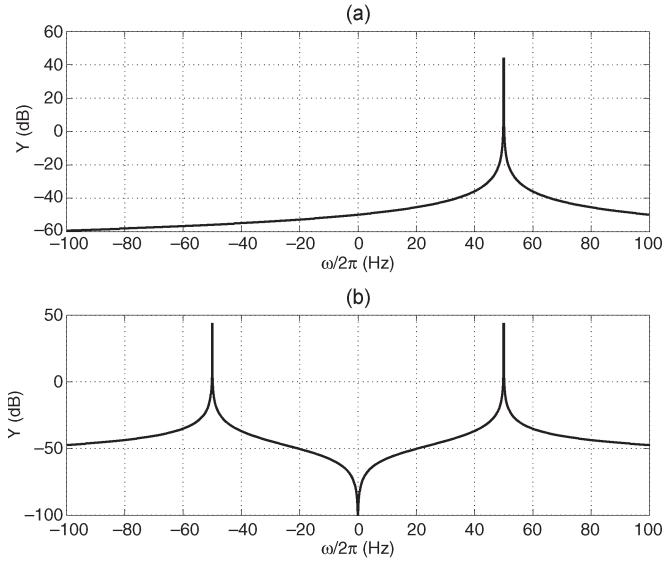

Fig. 3. Frequency response (magnitude). (a) ROGI. (b) SOGI.

In many current controllers, SOGIs are used as a basic building block. The SOGI is described by

$$\vec{y}^{\alpha\beta} = \frac{2p}{p^2+\omega_0^2}\vec{u}^{\alpha\beta}. \tag{4}$$

Fig. 3(b) shows the SOGI frequency response (magnitude). Note that, unlike the ROGI, that provides infinite gain only to a positive sequence input vector of frequency ω_0, the SOGI provides infinite gain for both positive and negative sequence input vectors of frequency ω_0. In addition, it must be noted that the SOGI (4) is a second-order equation, which requires four states to be implemented (two for each $\alpha\beta$ axis), whereas the ROGI (2) requires only two states (one for each $\alpha\beta$ axis). The lesser number of states of the ROGI against the SOGI's and the close relation between both are the reasons why, in this paper, (2) is named ROGI. In addition, note that with two ROGIs a SOGI can be constructed

$$\vec{y}^{\alpha\beta} = \left[\frac{1}{p-j\omega_0}+\frac{1}{p+j\omega_0}\right]\vec{u}^{\alpha\beta} = \frac{2p}{p^2+\omega_0^2}\vec{u}^{\alpha\beta}. \tag{5}$$

Both SOGIs and ROGIs are integrators that provide infinite gain to certain sinusoidal signals, but the ROGI requires fewer states in its implementation (less computational load) and provides discrimination between positive and negative sequence signals, a feature that is attractive, as will be shown in the next section. In three-phase current controllers implemented in the stationary reference frame, requiring only tracking of positive sequence signals in harmonic-free balanced grids [16]–[18], the use of a ROGI is computationally more efficient than using a SOGI. In contrast, it is of note that the SOGI can be adapted to single-phase systems, while the ROGI concept comes naturally for three-phase systems.

The ROGI can also be used in the stationary reference frame to implement a current controller with the same harmonic compensation capability as those used in [21]–[23]. There, several SOGIs with resonant frequency at $6n\omega_0$ are implemented in a reference frame rotating at frequency ω_0. To verify this ROGI feature with an example, note that the sum of two ROGIs tuned to harmonics $-5\omega_0$ and $+7\omega_0$ produces

$$\vec{y}^{\alpha\beta} = \left[\frac{1}{p+j5\omega_0}+\frac{1}{p-j7\omega_0}\right]\vec{u}^{\alpha\beta}. \tag{6}$$

Transforming this equation to the dq rotating reference frame by $\vec{u}^{\alpha\beta} = e^{j\theta}\vec{u}^{dq}$ and $\vec{y}^{\alpha\beta} = e^{j\theta}\vec{y}^{dq}$, it results

$$\vec{y}^{dq} = \left[\frac{1}{p-j6\omega_0}+\frac{1}{p+j6\omega_0}\right]\vec{u}^{dq} = \frac{2p}{p^2+(6\omega_0)^2}\vec{u}^{dq} \tag{7}$$

which represents a SOGI with resonant frequency $6\omega_0$, acting in the dq rotating reference frame. The clear advantage of implementing (6) instead of (7) is of computational nature, because (6), in spite of having the same number of states as (7), avoids the use of coordinate transformations.

III. Proposed ROGI-Based Controller

In this section, a current controller based on the ROGI structure described in the previous section is proposed. In what follows, it is assumed that the grid voltage is described by the following space vector:

$$\vec{v}_s^{\alpha\beta} = V_{1+}e^{j\omega_0 t} + \vec{v}_h^{+} + V_{1-}e^{-j\omega_0 t} + \vec{v}_h^{-} \tag{8}$$

where V_{1+} and V_{1-} are complex phasors that represent the positive and negative fundamental components of the grid voltage, $\vec{v}_h^{+}$ is a complex space vector that takes into account the harmonic contents associated to V_{1+}, and $\vec{v}_h^{-}$ is a complex space vector that takes into account those associated to V_{1-}

$$\vec{v}_h^{+} = \sum_n V_{(6n-1)-}e^{-j(6n-1)\omega_0 t} + V_{(6n+1)+}e^{j(6n+1)\omega_0 t} \tag{9}$$

$$\vec{v}_h^{-} = \sum_n V_{(6n-1)+}e^{j(6n-1)\omega_0 t} + V_{(6n+1)-}e^{-j(6n+1)\omega_0 t} \tag{10}$$

where $V_{(6n+1)+}$, $V_{(6n+1)-}$, $V_{(6n-1)+}$, and $V_{(6n-1)-}$ are complex phasors. Usually, in normal operation conditions (NOCs), the grid voltage unbalance is lesser than 3% [40], so the $\vec{v}_h^{-}$ term (10) is negligible. Harmonic pollution present in $\vec{v}_s^{\alpha\beta}$ is mainly due to the term $\vec{v}_h^{+}$, which is composed of negative sequence components of frequency $5\omega_0, 11\omega_0, (6n-1)\omega_0$, $n>0$, and positive sequence components of frequency $7\omega_0, 13\omega_0,$ and $(6n+1)\omega_0$. The term $\vec{v}_h^{-}$ is only noticeable in SVUC.

Fig. 4 shows the proposed current controller. The ac side circuit represents the connection inductors L, inserted between the grid voltage $\vec{v}_s^{\alpha\beta}$ and the VSC output $\vec{v}_i$ (see Fig. 1). The complex space vector $\vec{i}^{\alpha\beta}$ represents the injected grid current, and the signal $\vec{i}_{\mathrm{REF}}^{\alpha\beta}$ is the reference input to the current controller. This signal is synthesized to be proportional to the grid voltage

$$\vec{i}_{\mathrm{REF}}^{\alpha\beta} = g\vec{v}_s^{\alpha\beta} \tag{11}$$

where g is a signal that defines the average amount of power injected to the grid. This signal comes from the outer loop that regulates the bus voltage V_{DC}, a PI controller in Fig. 4. Because it is beyond the scope of this paper, in what follows, the effect of

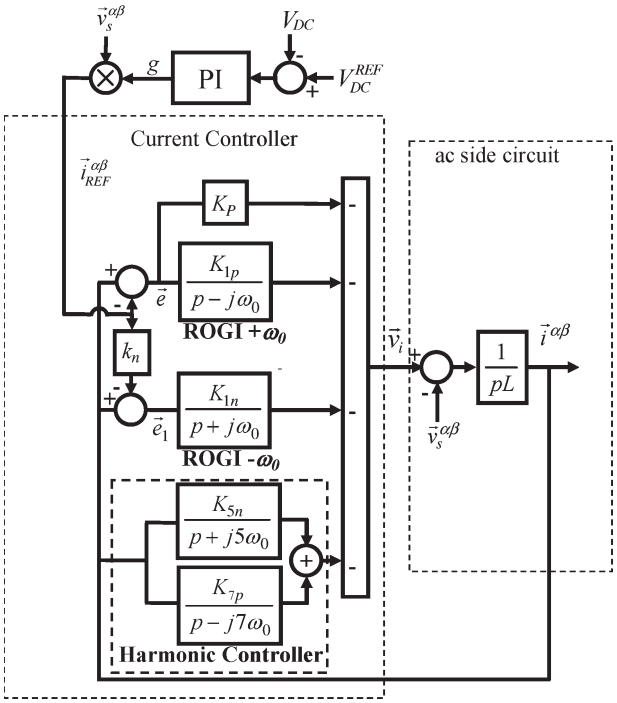

Fig. 4. Continuous time functional diagram of the proposed controller.

this outer control loop in the current controller is not included, and g is assumed to be a constant.

The controller is composed of two fundamental frequency ROGIs, resonating at $+\omega_0$ and $-\omega_0$, and a harmonic controller, composed by ROGIs resonating at certain harmonic frequencies. In the case shown, only two ROGIs resonating at frequency $-5\omega_0$ and $+7\omega_0$ were included. In a practical situation, as many ROGIs as harmonics present in $\vec{v}_h^{+}$ to be canceled should be included. No ROGIs to cancel the harmonics present in $\vec{v}_h^{-}$ were included. Including them would not bring great benefits in NOC and increases the order of the controller. Furthermore, the effect of these additional ROGIs would only be noticeable in SVUC, which is a transient situation, since the DPGS should cease to operate a short time after the fault is detected (clearing time) [6]. The proposed controller has the same ability to reject disturbances and the same number of states as SOGI-based resonant controllers implemented in a synchronous reference frame rotating at frequency $+\omega_0$ [21]–[23]. The advantage of the proposed controller over these proposals is that, here, no coordinate change is used.

In what follows, two scenarios of operation of the DPGS will be shown: one of NOC, with low-voltage imbalance, and one of SVUC. The constant k_n present in Fig. 4 allows to select among three different strategies of instantaneous active power injection [34]. According to the number of ROGIs included in the harmonic controller, all three strategies are capable of producing sinusoidal currents.

A. Balanced Current Injection

In this case, $k_n = 0$ must be chosen. The controller ensures symmetrical currents, in phase with the fundamental positive sequence component of the grid voltage $\vec{v}_s^{\alpha\beta}$.

1) NOC: To understand the controller operation, note observing Fig. 4 that the current $\vec{i}^{\alpha\beta}$ cannot contain any components of frequencies $-\omega_0$, $-5\omega_0$ nor $+7\omega_0$ (in the general case neither $-(6n-1)\omega_0$ nor $+(6n+1)\omega_0$). This is because the ROGIs tuned at $-\omega_0$, $-5\omega_0$, and $+7\omega_0$ have infinite gain at these frequencies, and their inputs (for $k_n = 0$) are fed directly by $\vec{i}^{\alpha\beta}$. Note also that the error $e = \vec{i}^{\alpha\beta} - \vec{i}^{\alpha\beta}_{\mathrm{REF}}$ is fed at the input of a ROGI tuned at $+\omega_0$, so such an error cannot contain any component at this frequency. Both facts allow to infer that the current will exactly track the fundamental positive sequence component of $\vec{i}^{\alpha\beta}_{\mathrm{REF}}$, even when $\vec{i}^{\alpha\beta}_{\mathrm{REF}}$ is contaminated with components of frequencies $-\omega_0$, $-(6n-1)\omega_0$, or $+(6n+1)\omega_0$. These undesirable components are canceled out and do not appear in the $\vec{i}^{\alpha\beta}$ current. This fact is checked in the next section, obtaining the frequency response of the transfer functions between the inputs $i^{\alpha\beta}_{\mathrm{REF}}$ and $\vec{v}_s^{\alpha\beta}$ and the output current $\vec{i}^{\alpha\beta}$.

According to what has been explained, from (8)–(11), the current results in

$$\vec{i}^{\alpha\beta} = gV_{1+}e^{j\omega_0 t}. \tag{12}$$

Using this equation and (8), after some algebraic manipulation, the instantaneous active power injected can be found to be

$$\begin{aligned} p_o &= \mathrm{Re}\left[\vec{v}_s^{\alpha\beta}(\vec{i}^{\alpha\beta})^*\right] \\ &= g|V_{1+}|^2 + g\mathrm{Re}\left[V_{1-}V_{1+}^* e^{-j2\omega_0 t}\right] \\ &\quad + g\mathrm{Re}\left[V_{1+}^* e^{-j\omega_0 t}\left(\vec{v}_h^{+} + \vec{v}_h^{-}\right)\right] \end{aligned} \tag{13}$$

where $*$ stands for conjugate complex. Note that, with this strategy, the VSC injects constant instantaneous active power to the network only through the positive component of $\vec{v}_s^{\alpha\beta}$, while the other voltage components produce pulsed-power terms that do not contribute to net energy exchange.

2) SVUC: The fundamental frequency component of the current is still balanced, which reduces the current stress on the converter switches. However, because in SVUC the term $\vec{v}_h^{-}$ in (8) becomes appreciable, the current does appear contaminated by harmonics of sequences $+(6n-1)\omega_0$ and $-(6n+1)\omega_0$ present in $\vec{v}_h^{-}$. These sequences cannot be compensated by the ROGIs included in the controller.

B. Constant Power Injection

In this case, $k_n = -1$ must be chosen. The controller ensures $2\omega_0$ ripple-free instantaneous active power injection.

1) NOC: The analysis of the controller behavior is identical to the previous case, noting only that, in this case, the signal $\vec{e}_1 = \vec{i}^{\alpha\beta} + \vec{i}^{\alpha\beta}_{\mathrm{REF}}$ cannot contain any component of frequency $-\omega_0$, because this signal is exciting a ROGI tuned to that frequency. Accordingly, $\vec{i}^{\alpha\beta}$ should now contain, in addition to the previous case, the negative sequence component of fundamental frequency present in $-\vec{i}^{\alpha\beta}_{\mathrm{REF}}$, whose value is $-gV_{1-}e^{-j\omega_0 t}$. Thus, in this case, the current results in

$$\vec{i}^{\alpha\beta} = g(V_{1+}e^{j\omega_0 t} - V_{1-}e^{-j\omega_0 t}). \tag{14}$$

The instantaneous active power exchanged is now

$$\begin{aligned} p_o &= \mathrm{Re}\left[\vec{v}_s^{\alpha\beta}(\vec{i}^{\alpha\beta})^*\right] \\ &= g|V_{1+}|^2 - g|V_{1-}|^2 \\ &\quad + g\mathrm{Re}\left[\left(V_{1+}^* e^{-j\omega_0 t} - V_{1-}^* e^{j\omega_0 t}\right)\left(\vec{v}_h^{+} + \vec{v}_h^{-}\right)\right]. \end{aligned} \quad (15)$$

Note that, in this case, when $\vec{v}_s^{\alpha\beta}$ is contaminated with negative sequence components, the pulsed component at frequency $2\omega_0$, present in (13), does not appear in the instantaneous active power. Eliminating this ripple increases the lifetime of the capacitor of the dc bus and reduces the risks of the bus voltage falling below the minimum acceptable level for operation. In a wind generation system, the torque pulsations on the axis of the machine produced by the pulsating power exchange are eliminated [41]. Note also in (15) that the VSC injects energy into the grid through the positive sequence component V_{1+} and drains energy from the grid through the negative sequence component V_{1-}. The price paid for eliminating the $2\omega_0$ ripple in the injected power is to decrease the ratio of injected power per ampere.

2) SVUC: As in the balanced current injection (BCI) strategy under SVUC, the currents are contaminated with harmonics, but unlike it, they are no longer balanced.

It is noteworthy that at a short circuit between two phases, in which the system becomes equivalent to a single-phase system, the system responds by simply canceling the current through the phase without fault, because in a one-phase system it is impossible to inject $2\omega_0$ ripple-free instantaneous active power. In this case, a reactive current circulating between the two phases in failure appears, which is not reflected on the phase without fault.

C. Maximum Power Injection

In this case, $k_n = 1$ must be chosen. The controller ensures currents in phase with the fundamental frequency component of $\vec{v}_s^{\alpha\beta}$, maximizing this way the instantaneous active power injection. The strategy used here is related to that used in [42] in a SOGI-based controller, where each harmonic requires four states to be canceled.

1) NOC: The signal $\vec{e}_1$ is now $\vec{e}_1 = \vec{i}^{\alpha\beta} - \vec{i}_{\mathrm{REF}}^{\alpha\beta}$, so it can be inferred by reasoning in a similar way to the previous case that $\vec{i}^{\alpha\beta}$ should now contain the negative sequence component of fundamental frequency present in $\vec{i}_{\mathrm{REF}}^{\alpha\beta}$ whose value is $gV_{1-}e^{-j\omega_0 t}$. It is, thus, the reason that the current in this case results in

$$\vec{i}^{\alpha\beta} = g(V_{1+}e^{j\omega_0 t} + V_{1-}e^{-j\omega_0 t}). \quad (16)$$

The instantaneous active power exchanged is now

$$\begin{aligned} p_o &= \mathrm{Re}\left[\vec{v}_s^{\alpha\beta}(\vec{i}^{\alpha\beta})^*\right] \\ &= g|V_{1+}|^2 + g|V_{1-}|^2 \\ &\quad + g\mathrm{Re}\left[V_{1+}V_{1-}^* e^{j2\omega_0 t} + V_{1-}V_{1+}^* e^{-j2\omega_0 t}\right] \\ &\quad + g\mathrm{Re}\left[\left(V_{1+}^* e^{-j\omega_0 t} + V_{1-}^* e^{j\omega_0 t}\right)\left(\vec{v}_h^{+} + \vec{v}_h^{-}\right)\right]. \end{aligned} \quad (17)$$

In this case, the VSC injects energy to the network through both components V_{1+} and V_{1-} of the grid voltage.

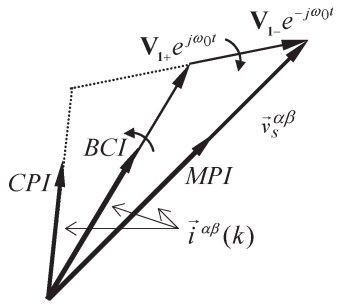

Fig. 5. Locus of the space vectors $\vec{i}^{\alpha\beta}$ and $\vec{v}_s^{\alpha\beta}$ for the three strategies (harmonic-free case).

2) SVUC: As in the BCI and CPI strategies under SVUC, the currents have harmonic content. Note comparing (17) with (13) that the $2\omega_0$ pulsating term has increased with respect to the BCI strategy. This is particularly appreciable in SVUC, where the term V_{1-} becomes apparent. The price paid for increasing the ratio of injected power per ampere is to increase the second harmonic ripple on the dc bus.

Fig. 5 shows the locus of the space vectors $\vec{i}^{\alpha\beta}$ and $\vec{v}_s^{\alpha\beta}$ for the three strategies, in the harmonic-free case. Note that, in the maximum power injection (MPI) case, the vectors are always in phase, nullifying the instantaneous reactive power injected. In contrast, the BCI and CPI strategies produce reactive power exchange between the VSC and the network, degrading in this way the ratio of injected power per ampere.

Remark 1: Note in Fig. 5 that an intermediate value of k_n between -1 and 1 can produce a linear combination of strategies.

Remark 2: The online exchange between strategies may be useful in certain situations, in addition to those outlined in [34]. For example, in systems operating in NOC, it is in general desirable to inject through the MPI strategy to maximize the injected power per ampere, reducing resistive losses and increasing the overall efficiency of the distributed system. When the imbalance exceeds normal limits, it may be desirable to inject through the BCI or CPI strategies (or through a linear combination of strategies). In a photovoltaic system, for example, it is a known fact that the ripple in the dc bus moves the operation point of the solar panel around the maximum power point (MPP), which affects the MPP tracking capability of the system and, therefore, the overall efficiency. When the imbalance is large, the MPI strategy may not be the most appropriate for this case. On SVUC, it may be desirable to switch to the CPI strategy, in order to minimize the stress on the dc bus capacitor and ensure that the dc voltage does not fall below the allowable minimum operating voltage.

IV. Discrete-Time Implementation and System Analysis

Instead of starting from designing the controller in the continuous time domain and then proceeding to its discretization [43], in this paper, the controller design is done in the discrete-time domain, based on the state variable technique. Doing this allows easy tuning of the controller and takes into account the DSP delay as part of the system to stabilize, which ensures proper controller operation even for large processing delays.

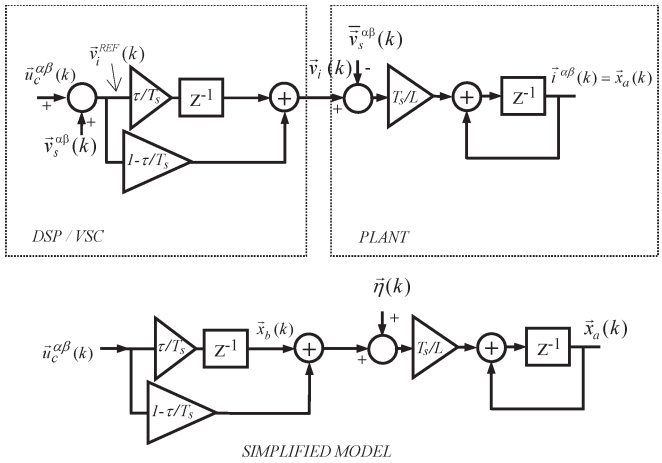

Fig. 6. Discrete-time model of the plant and processing delay.

A. Digital Implementation

Fig. 6 (top right side) shows the discrete-time model of the plant, consisting of the inductor L connected between the network and the VSC. In this figure, $\vec{v}_s^{\alpha\beta}(k)$ denotes the average of $\vec{v}_s^{\alpha\beta}(t)$ in the interval $kT_s \leq t < (k+1)T_s$, where T_s is the sampling time, and $\vec{v}_i(k)$ is the VSC average output voltage, averaged on the same interval. In the DSP/VSC section (Fig. 6, top left side), the processing delay $\tau \leq T_s$ introduced by the DSP between the output voltage $\vec{v}_i(k)$ and the reference voltage provided to the pulsewidth modulation (PWM) modulator [denoted $\vec{v}_i^{\mathrm{REF}}(k)$] is modeled by

$$\vec{v}_i(k) = \left(1 - \frac{\tau}{T_s}\right)\vec{v}_i^{\mathrm{REF}}(k) + \left(\frac{\tau}{T_s}\right)\vec{v}_i^{\mathrm{REF}}(k-1). \quad (18)$$

For simplicity, this modulator was not included in the figure and was supposed of unity gain. Note that $\vec{v}_i(k)$ is modeled as the average between the actual PWM modulator input $\vec{v}_i^{\mathrm{REF}}(k)$ and the previous input $\vec{v}_i^{\mathrm{REF}}(k-1)$, weighted by the relation τ/T_s. For $\tau = 0$, it results in $\vec{v}_i(k) = \vec{v}_i^{\mathrm{REF}}(k)$, and for $\tau = T_s$, it results in $\vec{v}_i(k) = \vec{v}_i^{\mathrm{REF}}(k-1)$.

As Fig. 6 shows, the PWM reference $\vec{v}_i^{\mathrm{REF}}(k)$ is conformed by a feedforward term $\vec{v}_s^{\alpha\beta}(k)$, which is the sampled value of $\vec{v}_s^{\alpha\beta}(t)$ at time kT_s, plus the signal $\vec{u}_c^{\alpha\beta}(k)$, which is the signal that will be synthesized by full state feedback, as detailed hereinafter. The feedforward term is introduced to partially cancel the effect of $\bar{\vec{v}}_s^{\alpha\beta}(k)$ on the output $\vec{i}^{\alpha\beta} \equiv x_a(k)$. This feedforward term, although not vital to the controller operation, is introduced to improve the dynamic response of the system to possible changes in the grid voltage. Fig. 6 (bottom) shows a simplified block diagram of the so far explained system, where

$$\vec{\eta}(k) = \frac{\tau}{T_s}\vec{v}_s^{\alpha\beta}(k-1) + \left(1 - \frac{\tau}{T_s}\right)\vec{v}_s^{\alpha\beta}(k) - \bar{\vec{v}}_s^{\alpha\beta}(k) \quad (19)$$

can be considered as a perturbation term. The term can be found by algebraic manipulation of (18), by noting that $\vec{v}_i^{\mathrm{REF}}(k) = \vec{u}_c^{\alpha\beta}(k) + \vec{v}_s^{\alpha\beta}(k)$.

The digital ROGI implementation will now be explained. As the poles of a continuous system are mapped to a discrete system by the transformation $z = e^{sT_s}$, the discrete-time system described by

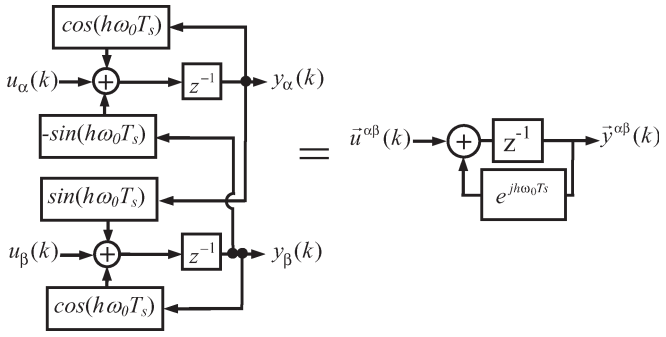

Fig. 7. Discrete-time implementation of a continuous system with a pole in $jh\omega_0$.

$$G_h(z) = \frac{\vec{y}^{\alpha\beta}(z)}{\vec{u}^{\alpha\beta}(z)} = \frac{1}{z - e^{jh\omega_0 T_s}} \quad (20)$$

is the discrete-time version of a continuous time system with a pole in $jh\omega_0$. Fig. 7 shows the $\alpha\beta$ implementation of (20). In what follows, (20) will be used to implement the controller.

Fig. 8 shows the proposed current controller responsible for synthesizing the signal $\vec{u}_c^{\alpha\beta}(k)$ in Fig. 6. It is composed of the resonant sections (20), according to the guidelines presented in the preceding section. Again, for simplicity, the harmonic controller includes only two ROGIs, resonating at frequencies $-5\omega_0$ and $+7\omega_0$, but the design procedure detailed in what follows is general and allows to include more resonant sections. Note in Fig. 8 the presence of the signal $x_b(k) = (\tau/T_s)\vec{u}_c^{\alpha\beta}(k-1)$, defined in Fig. 6 (bottom). This signal must be included in the controller, in order to perform full state feedback. The processing delay is thus included as an additional state of the system to stabilize.

Considering, for the time being, $\vec{i}_{\mathrm{REF}}^{\alpha\beta}$ and $\vec{\eta}(k)$ as two external perturbations that do not affect the closed-loop stability, then the open-loop system ($K = K_P = K_{1p} = \ldots = K_{7p} = 0$) composed by Figs. 6 and 8 can be described as

$$\mathbf{x}(k+1) = \mathbf{A}\mathbf{x}(k) + \mathbf{B}\vec{u}_c^{\alpha\beta}(k) \quad (21)$$

where $\mathbf{A} \in \mathbb{C}^{(2+r)\times(2+r)}$ (r being the number of ROGIs included in the controller)

$$\mathbf{A} = \begin{bmatrix} 1 & \frac{T_s}{L} & 0 & 0 & 0 & \cdots & 0 \\ 0 & 0 & 0 & 0 & 0 & \cdots & 0 \\ 1 & 0 & e^{j\omega_0 T} & 0 & 0 & \cdots & 0 \\ 1 & 0 & 0 & e^{-j\omega_0 T} & 0 & \cdots & 0 \\ 1 & 0 & 0 & 0 & e^{-j5\omega_0 T} & \cdots & 0 \\ \vdots & \vdots & \vdots & \vdots & \vdots & \ddots & 0 \\ 1 & 0 & 0 & 0 & 0 & 0 & e^{\pm jn\omega_0 T} \end{bmatrix}$$

$$\mathbf{B} = \begin{bmatrix} \frac{(T_s-\tau)}{L} & \frac{\tau}{T_s} & 0 & \ldots 0 \end{bmatrix}^T$$

$$\mathbf{x} = \begin{bmatrix} x_a & x_b & x_{1p} & x_{1n} & x_{5n} & \ldots \end{bmatrix}^T.$$

The signal $\vec{u}_c^{\alpha\beta}(k)$ in Fig. 8 is synthesized as a linear combination of the states $\vec{x}_b, \vec{x}_a, \vec{x}_{1p}, \ldots, \vec{x}_{7p}$, through appropriate

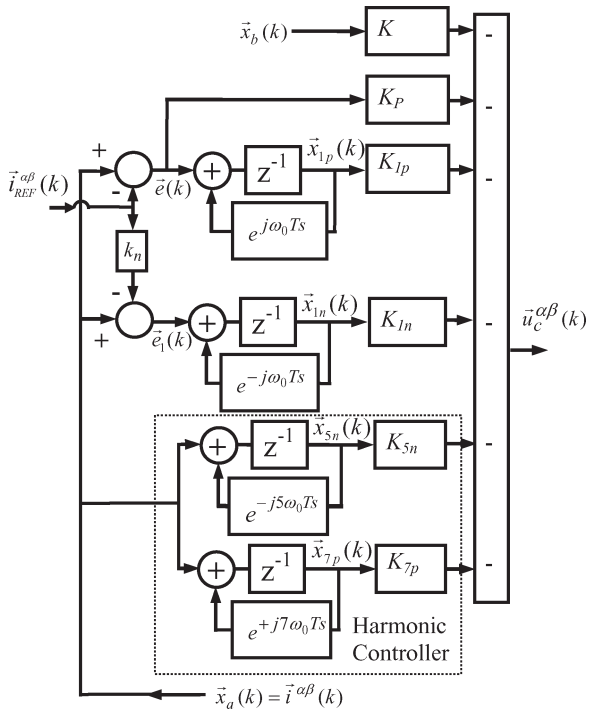

Fig. 8. Controller implementation in the discrete-time domain.

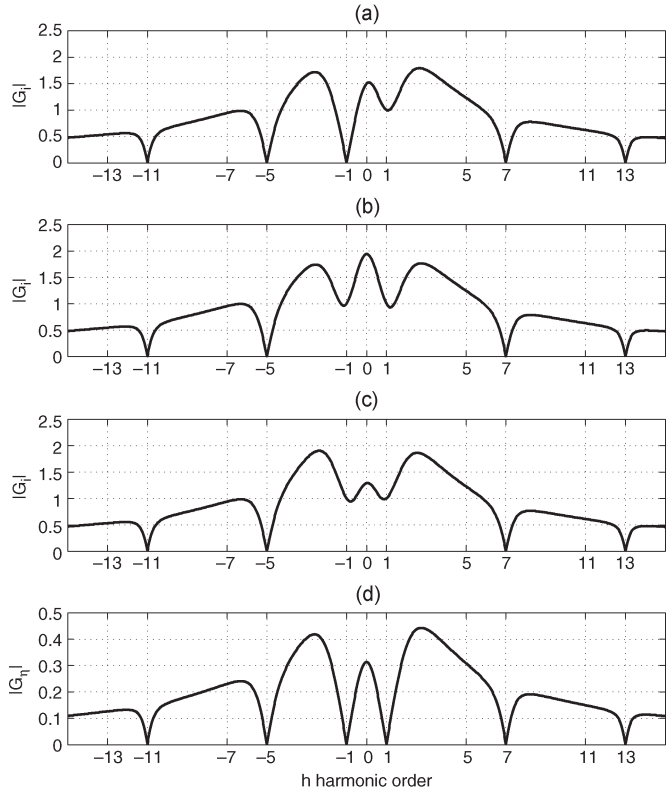

Fig. 9. Frequency response: $|G_i(e^{j\omega T_s})|$, $|G_\eta(e^{j\omega T_s})|$. (a) BCI ($k_n = 0$). (b) CPI ($k_n = -1$). (c) MPI ($k_n = 1$). (d) Grid disturbance rejection capability.

feedback gains $K, K_P, K_{1p}, \ldots, K_{7p}$. By imposing the feedback law

$$\vec{u}_c^{\alpha\beta}(k) = -\mathbf{L^T}\mathbf{x}(k) \tag{22}$$

with $\mathbf{L^T} = [K_P\ K\ K_{1p}\ K_{1n} \ldots\ldots K_{7p}]$, the closed-loop system results in

$$\mathbf{x}(k+1) = (\mathbf{A} - \mathbf{BL^T})\mathbf{x}(k) = \mathbf{A_{CL}}\mathbf{x}(k) \tag{23}$$

where $\mathbf{A_{CL}} = \mathbf{A} - \mathbf{BL^T}$. By using any tool from control theory of linear systems, it is possible to choose the gain vector $\mathbf{L}$ in order to achieve the desired closed-loop behavior of the system. For example, since the system is controllable, Ackermann's formula or any other pole placement technique can be applied, to locate the eigenvalues of $\mathbf{A_{CL}}$ on appropriate values. Placing the $2 + r$ eigenvalues at the origin, for example, dead beat response can be achieved, where the output converges to the desired value in $2 + r$ steps. Another possible strategy to choose $\mathbf{L}$ is the use of linear quadratic regulator (LQR) theory. This strategy frees the designer from choosing the location of the closed-loop poles and generally produces a robust closed-loop system. In LQR theory, $\mathbf{L}$ must be chosen to minimize the cost function

$$J = \sum_{k=0}^{\infty} \mathbf{x^H}(k)\mathbf{Q}\mathbf{x}(k) + R\left|\vec{u}_c^{\alpha\beta}(k)\right|^2 \tag{24}$$

where $(.)^{\mathbf{H}}$ denotes transpose conjugate, $\mathbf{Q} \in \mathbb{C}^{(2+r)\times(2+r)}$ is a Hermitian matrix, and $R \in \mathbb{R}$ denotes weighting factors. The solution is obtained by solving Riccati's algebraic equation [44].

Note that, for computing the feedback gains $\mathbf{L}$, the constant k_n present in Fig. 8, necessary for selecting one of the three described active power injection strategies, is not involved. This enables to choose online the strategy that best suits the DPGS current operating condition, simply by choosing the right k_n value for computing the $\vec{e}_1$ signal in Fig. 8.

B. System Analysis

Consider now the presence of the inputs $\vec{i}^{\alpha\beta}_{\mathrm{REF}}$ and $\vec{\eta}(k)$. The closed-loop system is described as

$$\mathbf{x}(k+1) = \mathbf{A_{CL}}\mathbf{x}(k) + \mathbf{B_i}\vec{i}^{\alpha\beta}_{\mathrm{REF}}(k) + \mathbf{B_\eta}\vec{\eta}^{\alpha\beta}(k) \tag{25}$$

$$\vec{i}^{\alpha\beta}(k) = \mathbf{C}\mathbf{x}(k) \tag{26}$$

where

$$\mathbf{B_i} = \left[\frac{K_P(T_s-\tau)}{L}\ \frac{\tau K_P}{T_s}\ -1\ -k_n\ 0 \ldots 0\right]^T$$

$$\mathbf{B_\eta} = \left[\frac{T_s}{L}\ 0\ 0\ \ldots\ 0\right]^T$$

$$\mathbf{C} = [1\ 0\ 0\ \ldots\ 0]^T.$$

Using the Z transform, the transfer functions $G_i(z) = \vec{i}^{\alpha\beta}(z)/\vec{i}^{\alpha\beta}_{\mathrm{REF}}(z)$ and $G_\eta(z) = \vec{i}^{\alpha\beta}(z)/\vec{\eta}^{\alpha\beta}(z)$ for the closed-loop system (25) and (26) are found. The frequency response of each can be obtained using the mapping $z = e^{j\omega T_s}$. These frequency responses (evaluated for the three proposed strategies) are shown in Figs. 9 and 10 for a typical current controller composed of $r = 6$ resonant sections tuned at frequencies $h\omega_0$,

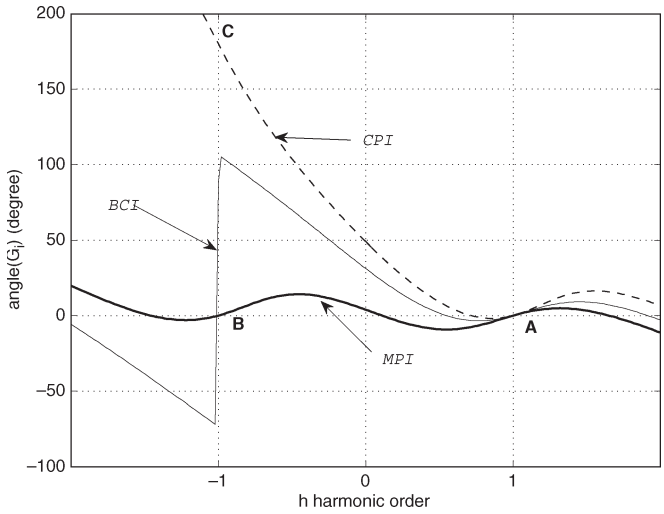

Fig. 10. Frequency response: $\arg[G_i(e^{j\omega T_s})]$.

$h = +1, -1, -5, +7, -11$, and -13, designed for $L = 3$ mH and $\tau = T_s = 200$ μs. Note in Fig. 9(a)–(c) that $G_i(z)$ has zeros at harmonic orders $h = -11, -5, 7, 13$, meaning that the controller removes from $\vec{i}^{\alpha\beta}$, as explained before, all the components present in $\vec{i}^{\alpha\beta}_{\rm REF} = g\vec{v}^{\alpha\beta}_s$ that have those frequencies. Note also that the three transfer functions present unity gain and zero phase shift for the sequence $h = 1$ (the latter is shown in Fig. 10, point A). This confirms that $\vec{i}^{\alpha\beta}$ includes an exact copy of the fundamental positive sequence component of $\vec{i}^{\alpha\beta}_{REF}$.

As was said, the different behavior between the three controllers lies in the treatment done on the negative sequence component $h = -1$ present in $\vec{i}^{\alpha\beta}_{\rm REF}$. Whereas the BCI strategy eliminates such component from the output [zero at $h = -1$ in Fig. 9(a)], the CPI and MPI strategies include it in the output without magnitude change [unity gain at $h = -1$ in Fig. 9(b)–(c)]. In the MPI strategy, it appears without phase change (point B of Fig. 10), and in the CPI strategy, it appears with a phase change of 180° (point C of Fig. 10).

Fig. 9(d) shows the controller ability to reject all components at frequencies $h\omega_0$, $h = -11, -5, -1, 1, 7,$ and 13 present in the disturbance $\vec{\eta}^{\alpha\beta}$. Note that the transfer function $G_\eta(z)|_{z=e^{j\omega T_s}}$ has zeros at such frequencies, confirming [alongside (19)] that the presence of these components in $\vec{v}^{\alpha\beta}_s$ does not affect the $\vec{i}^{\alpha\beta}$ current.

V. Simulation Results

A system similar to that shown in Fig. 1 was simulated. Instead of an inductor, an LCL ripple filter was used as output filter ($L_1 = 2.4$ mH VSC side, $L_2 = 2.9$ mH line side, and $C = 4.7$ μF with equivalent series resistance of 4.7 Ω). In order to evaluate the performance of the controller to unmodeled dynamics, the dynamics of this LCL filter are not considered in the controller design [45]. As the parallel branch of the LCL filter is practically an open circuit at fundamental frequency, the controller is designed considering $L = L_1 + L_2$. The space vector PWM (SV-PWM) was implemented with a 20-kHz carrier frequency, the sampling period was $T_s = 200$ μs, and the processing delay was $\tau = T_s$. For the simulations, a low sampling rate and a large processing delay were used, in order to verify the good performance of the proposed algorithm in highly adverse conditions. In practical applications involving modern fixed-point DSPs (as the one used to obtain the experimental results of this paper), these conditions are often more relaxed.

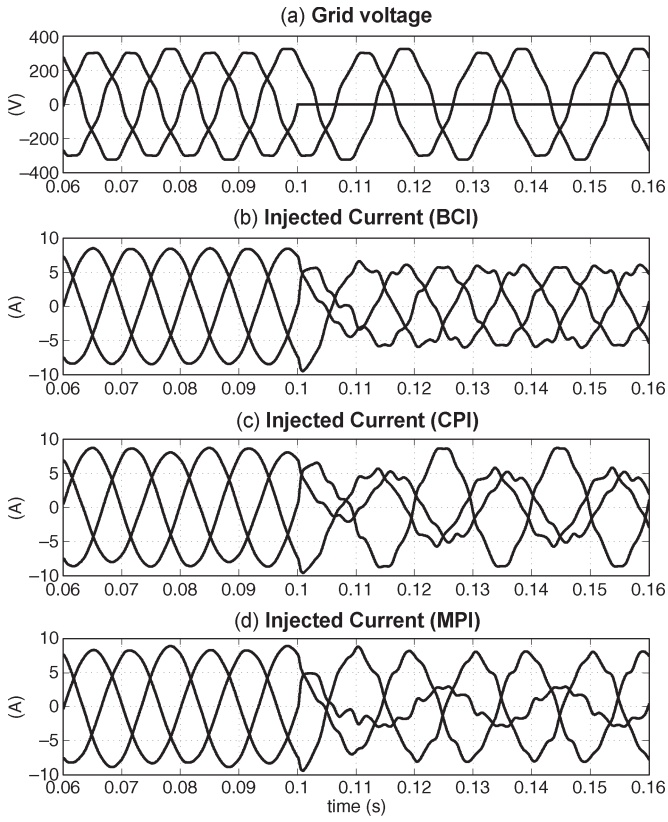

Fig. 11. NOC and SVUC waveforms. (a) Phase voltages. (b)–(d) Injected currents.

First-order antialiasing filters in the measured signals were included (2.34-kHz cutoff frequency). The current sensors were saturated at ±15 A. The dc bus voltage was 600 V. The grid voltage (220 V rms per phase) was contaminated by harmonics of orders 5th (3.5%), 7th (3.5%), 11th (1%), and 13th (0.25%). The controller was designed with ROGIs tuned at frequencies $h\omega_0$, $h = +1, -1, -5, +7, -11$, and $+13$ using the LQR method, with $R = 10$, and $Q = \mathrm{diag}\,[10\ 10\ 1\ 1\ 1\ 1\ 1\ 1]$, where diag stands for diagonal matrix.

Fig. 11 shows the phase voltages. As the simulated dc bus voltage is assumed to come from a constant power source, the control loop of the bus voltage was not implemented, and $g = 0.027\ \Omega^{-1}$ was imposed in (11). During $(t \leq 0.1$ s), the three controllers operate in NOC, with a voltage imbalance of 5%. During $(t > 0.1$ s), the three controllers are subject to SVUC produced by a short circuit between one phase and neutral. In NOC, the three controllers produce sinusoidal currents with very low harmonic content (THD $= 0.88\%$). In SVUC, the BCI controller is the only one that produces balanced currents. Note that, in SVUC, the currents synthesized by the three controllers are contaminated with harmonics. These harmonics are caused by the grid voltage components at $h = +5, -7, +11,$ and -13, which become significant in SVUC and cannot be rejected by

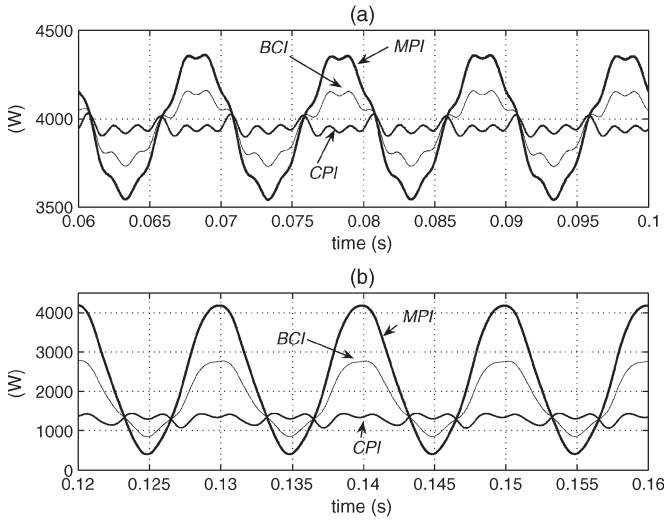

Fig. 12. Injected instantaneous active power. (a) Injected power (NOC). (b) Injected power (SVUC).

the controller. As explained before, these sequences can be canceled out if additional ROGIs are provided to the controller. Note, however, that the improvement of the THD in NOC would be negligible and would require, in this case, increasing the system complexity from 16 states to 24 states. This is a major complication to improve an occasional situation of very short duration, as is the DPGS operation in SVUC.

Fig. 12 shows the instantaneous active power injected. Note that the CPI strategy is the only one that eliminates the $2\omega_0$ power ripple, even during SVUC.

With the chosen $g = 0.027\ \Omega^{-1}$ value and $V_{1-} = 0.05V_{1+}$ and $|V_{1+}| = 380$ V, according to (13), the twice fundamental frequency ripple using the BCI strategy is around 194 W, whereas using the MPI strategy, according to (17), this value doubles. These facts are evidenced in Fig. 12.

VI. Experimental Results

Fig. 13 shows the experimental setup. A three-phase isolation transformer in connection DY1 with 132/380 V, 50 Hz, and 6 kVA was used. The available measurements were the currents i_{sa} and i_{sb}, the bus voltage $V_{\rm DC}$, and the line voltages V_{ca} and V_{cb}. The VSC bus voltage was 400 V. An LC ripple filter, whose parameters are shown in Fig. 13, was used. The primary leakage equivalent inductance (VSC side) of the transformer was 120 μH. The SVUC was caused by shorting one phase of the transformer secondary to the neutral grid point, by means of a selector switch S (producing thus the condition $v_s = 0$). The controller was implemented with ROGIs tuned at $h\omega_0$, $h = +1, -1, -5, +7, -11, +13, -17, +19, -23, +25$. Due to the large controller bandwidth, the discrete-time model of the antialiasing current measurement filter was added to the plant model (Fig. 6). The cutoff frequency of this filter was 2.34 kHz. The system complexity was then of 26 states. The controller was implemented in a fixed-point DSP TMS320F2812. The SV-PWM was implemented with a 20-kHz carrier frequency, the sampling period was $T_s = 100\ \mu$s, and the processing

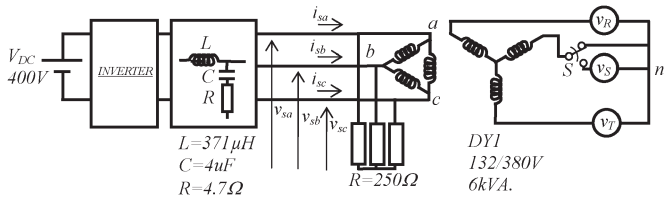

Fig. 13. Experimental setup.

Fig. 14. Implemented system.

delay was $\tau = T_s/2$. Fig. 14 shows the system hardware implementation.

Fig. 15 (top) shows the phase voltages applied (THD $= 4.5\%$). These voltages were measured with respect to the virtual neutral obtained from the three-phase balanced resistive load of 250 Ω shown in Fig. 13. Fig. 15 (bottom) shows the currents injected by the BCI strategy (resulting THD $= 2.5\%$). Both correspond to NOC. In this condition, the injected currents for the CPI and MPI strategies were virtually identical to those in Fig. 15, which is the reason why their graphs were omitted. Fig. 16 shows the measured phase voltages (top) along with the currents injected by each controller, in SVUC ($v_s = 0$). As expected, the BCI strategy is the only one that produces a balanced current set. Note that the MPI strategy yields currents in phase with the grid phase voltages. Also, as was predicted, all currents show harmonic contamination produced by the $\vec{v}_h^-$ term. Note that, to eliminate these harmonics, it would be necessary to add ROGIs tuned at $h\omega_0$, $h = +5, -7, +11, -13, +17, -19, +23, -25$ (or to use SOGIs), which would increase the system complexity from the

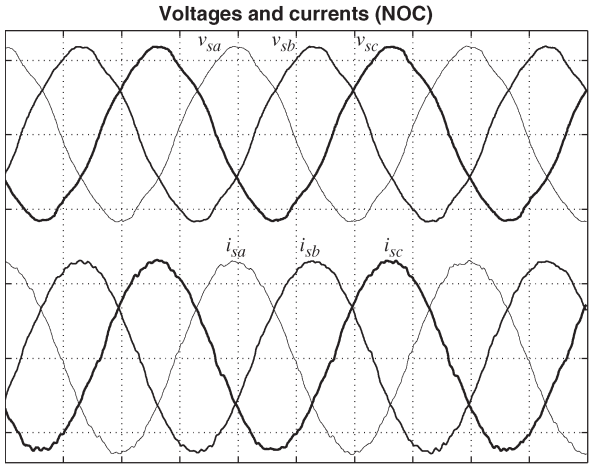

Fig. 15. Experimental results: Phase voltages and currents for the BCI strategy in NOC (vertical scale: 100 V/div, 25 A/div; horizontal scale: 5 ms/div).

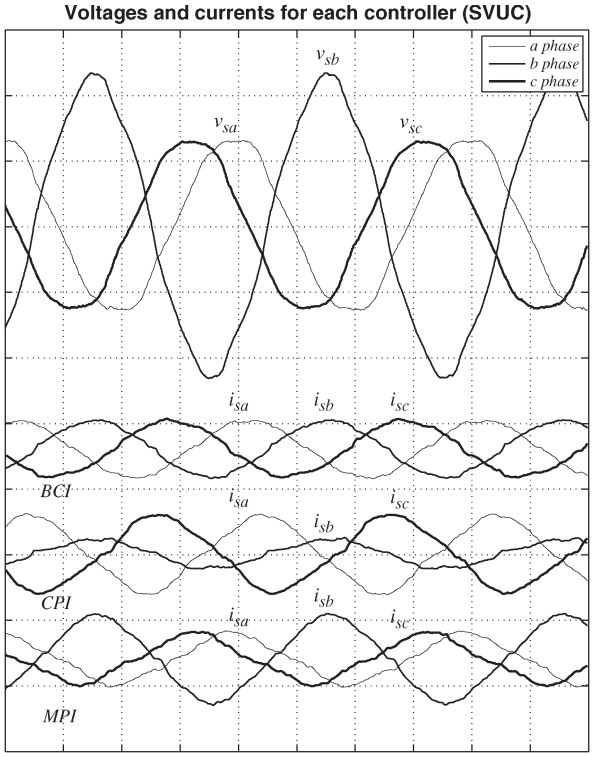

Fig. 16. Experimental results: Phase voltages and currents in SVUC (vertical scale: 50 V/div, 50 A/div; horizontal scale: 5 ms/div).

actual 26 states to 42 states. Nevertheless, the benefit in NOC would be negligible. Fig. 17 shows the power injected by each controller in SVUC. Note that the CPI strategy is the only one that is $2\omega_0$ ripple free.

VII. Conclusion

A ROGI-based current controller suitable for DPGS has been proposed. It is integrally implemented in the $\alpha\beta$ stationary reference frame, without using coordinate changes. The controller integrates the three basic functions required in DPGS: power quality, grid synchronization, and successful handling of severe voltage unbalanced conditions. It also allows to choose between

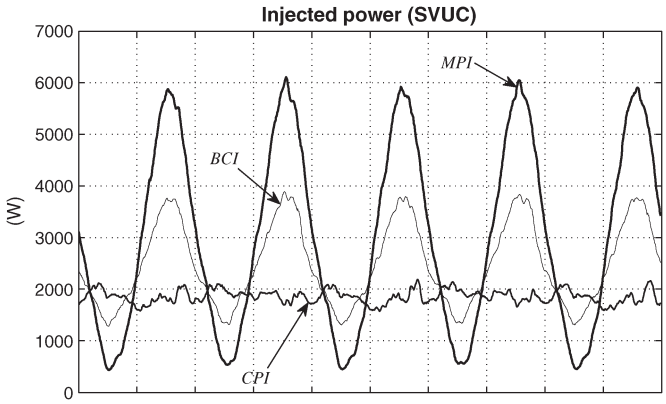

Fig. 17. Experimental results: Instantaneous injected power in SVUC (horizontal scale: 5 ms/div).

three different strategies for active power injection. This is all done with a very low computational effort and without requiring any dedicated synchronization algorithm. A discrete-time design of the controller, which includes the DSP processing delay as part of the plant model, was also presented. The methodology facilitates the tuning of controller gains, even when the number of controller states involved is high. The presented experimental results confirm the validity of the proposed algorithms.

References

[1] M. Cacciato, A. Consoli, R. Attanasio, and F. Gennaro, "Soft-switching converter with HF transformer for grid-connected photovoltaic systems," *IEEE Trans. Ind. Electron.*, vol. 57, no. 5, pp. 1678–1686, May 2010.

[2] J. Carrasco, L. Franquelo, J. Bialasiewicz, E. Galvan, R. Guisado, M. Prats, J. Leon, and N. Moreno-Alfonso, "Power-electronic systems for the grid integration of renewable energy sources: A survey," *IEEE Trans. Ind. Electron.*, vol. 53, no. 4, pp. 1002–1016, Jun. 2006.

[3] T. Zhou and B. Francois, "Energy management and power control of a hybrid active wind generator for distributed power generation and grid integration," *IEEE Trans. Ind. Electron.*, vol. 58, no. 1, pp. 95–104, Jan. 2011.

[4] H. Zhang and L. Tolbert, "Efficiency impact of silicon carbide power electronics for modern wind turbine full scale frequency converter," *IEEE Trans. Ind. Electron.*, vol. 58, no. 1, pp. 21–28, Jan. 2011.

[5] M. Mohr, W. Franke, B. Wittig, and F. Fuchs, "Converter systems for fuel cells in the medium power range—A comparative study," *IEEE Trans. Ind. Electron.*, vol. 57, no. 6, pp. 2024–2032, Jun. 2010.

[6] *IEEE Standard for Interconnecting Distributed Resources With Electric Power Systems*, IEEE Std. 1547-2003.

[7] C.-M. Ho, V. Cheung, and H.-H. Chung, "Constant-frequency hysteresis current control of grid-connected VSI without bandwidth control," *IEEE Trans. Power Electron.*, vol. 24, no. 11, pp. 2484–2495, Nov. 2009.

[8] Q. Zeng and L. Chang, "An advanced SVPWM-based predictive current controller for three-phase inverters in distributed generation systems," *IEEE Trans. Ind. Electron.*, vol. 55, no. 3, pp. 1235–1246, Mar. 2008.

[9] M. Kazmierkowski and L. Malesani, "Current control techniques for three-phase voltage-source PWM converters: A survey," *IEEE Trans. Ind. Electron.*, vol. 45, no. 5, pp. 691–703, Oct. 1998.

[10] A. Timbus, M. Liserre, R. Teodorescu, P. Rodriguez, and F. Blaabjerg, "Evaluation of current controllers for distributed power generation systems," *IEEE Trans. Power Electron.*, vol. 24, no. 3, pp. 654–664, Mar. 2009.

[11] F. Blaabjerg, R. Teodorescu, M. Liserre, and A. Timbus, "Overview of control and grid synchronization for distributed power generation systems," *IEEE Trans. Ind. Electron.*, vol. 53, no. 5, pp. 1398–1409, Oct. 2006.

[12] C. D. Schauder and R. Caddy, "Current control of voltage-source inverters for fast four-quadrant drive performance," *IEEE Trans. Ind. Appl.*, vol. IA-18, no. 2, pp. 163–171, Mar. 1982.

[13] P. Hsu and M. Behnke, "A three-phase synchronous frame controller for unbalanced load," in *Proc. 29th Annu. IEEE Power Electron. Spec. Conf.*, May 1998, vol. 2, pp. 1369–1374.

[14] S. Park, S.-B. Han, B.-M. Jung, S.-H. Choi, and H.-G. Jeong, "A current control scheme based on multiple synchronous reference frames for parallel hybrid active filter," in *Proc. 3rd Int. IPEMC*, 2000, pp. 218–223.
[15] T. M. Rowan and R. J. Kerkman, "A new synchronous current regulator and an analysis of current-regulated PWM inverters," *IEEE Trans. Ind. Appl.*, vol. IA-22, no. 4, pp. 678–690, Jul. 1986.
[16] Y. Sato, T. Ishizuka, K. Nezu, and T. Kataoka, "A new control strategy for voltage-type PWM rectifiers to realize zero steady-state control error in input current," *IEEE Trans. Ind. Appl.*, vol. 34, no. 3, pp. 480–486, May/Jun. 1998.
[17] D. Zmood, D. Holmes, and G. Bode, "Frequency domain analysis of three phase linear current regulators," in *34th Conf. Rec. IEEE IAS Annu. Meeting*, 1999, pp. 818–825.
[18] D. Zmood and D. Holmes, "Stationary frame current regulation of PWM inverters with zero steady-state error," *IEEE Trans. Power Electron.*, vol. 18, no. 3, pp. 814–822, May 2003.
[19] X. Yuan, W. Merk, H. Stemmler, and J. Allmeling, "Stationary-frame generalized integrators for current control of active power filters with zero steady-state error for current harmonics of concern under unbalanced and distorted operating conditions," *IEEE Trans. Ind. Appl.*, vol. 38, no. 2, pp. 523–532, Mar./Apr. 2002.
[20] G. Shen, X. Zhu, J. Zhang, and D. Xu, "A new feedback method for PR current control of LCL-filter-based grid-connected inverter," *IEEE Trans. Ind. Electron.*, vol. 57, no. 6, pp. 2033–2041, Jun. 2010.
[21] E. Blanco, E. Bueno, F. Espinosa, S. Cobreces, F. Rodriguez, and M. Ruiz, "Fast harmonics compensation in VSCs connected to the grid by synchronous-frame generalized integrators," in *Proc. IEEE ISIE*, 2005, vol. 2, pp. 751–755.
[22] R. Bojoi, G. Griva, V. Bostan, M. Guerriero, F. Farina, and F. Profumo, "Current control strategy for power conditioners using sinusoidal signal integrators in synchronous reference frame," *IEEE Trans. Power Electron.*, vol. 20, no. 6, pp. 1402–1412, Nov. 2005.
[23] M. Liserre, R. Teodorescu, and F. Blaabjerg, "Multiple harmonics control for three-phase grid converter systems with the use of PI-RES current controller in a rotating frame," *IEEE Trans. Power Electron.*, vol. 21, no. 3, pp. 836–841, May 2006.
[24] A. Timbus, R. Teodorescu, F. Blaabjerg, and M. Liserre, "Synchronization methods for three phase distributed power generation systems. An overview and evaluation," in *Proc. 36th IEEE Power Electron. Spec. Conf.*, 2005, pp. 2474–2481.
[25] F. Liccardo, P. Marino, and G. Raimondo, "Robust and fast three-phase PLL tracking system," *IEEE Trans. Ind. Electron.*, vol. 58, no. 1, pp. 221–231, Jan. 2011.
[26] P. Rodriguez, J. Pou, J. Bergas, J. Candela, R. Burgos, and D. Boroyevich, "Decoupled double synchronous reference frame PLL for power converters control," *IEEE Trans. Power Electron.*, vol. 22, no. 2, pp. 584–592, Mar. 2007.
[27] P. Rodriguez, A. Luna, I. Candela, R. Mujal, R. Teodorescu, and F. Blaabjerg, "Multiresonant frequency-locked loop for grid synchronization of power converters under distorted grid conditions," *IEEE Trans. Ind. Electron.*, vol. 58, no. 1, pp. 127–138, Jan. 2011.
[28] J. Svensson, M. Bongiorno, and A. Sannino, "Practical implementation of delayed signal cancellation method for phase-sequence separation," *IEEE Trans. Power Del.*, vol. 22, no. 1, pp. 18–26, Jan. 2007.
[29] G. Saccomando, J. Svensson, and A. Sannino, "Improving voltage disturbance rejection for variable-speed wind turbines," *IEEE Trans. Energy Convers.*, vol. 17, no. 3, pp. 422–428, Sep. 2002.
[30] P. W. Lehn and M. R. Iravani, "Discrete time modeling and control of the voltage source converter for improved disturbance rejection," *IEEE Trans. Power Electron.*, vol. 14, no. 6, pp. 1028–1036, Nov. 1999.
[31] H.-S. Song, I.-W. Joo, and K. Nam, "Source voltage sensorless estimation scheme for PWM rectifiers under unbalanced conditions," *IEEE Trans. Ind. Electron.*, vol. 50, no. 6, pp. 1238–1245, Dec. 2003.
[32] A. A. Girgis, W. Chang, and E. B. Makram, "Analysis of high-impedance fault generated signals using a Kalman filtering approach," *IEEE Trans. Power Del.*, vol. 5, no. 4, pp. 1714–1724, Oct. 1990.
[33] R. A. Flores, I. Y. H. Gu, and M. H. J. Bollen, "Positive and negative sequence estimation for unbalanced voltage dips," in *Proc. IEEE Power Eng. Soc. Gen. Meeting*, Jul. 2003, vol. 4, pp. 2498–2502.
[34] P. Rodriguez, A. Timbus, R. Teodorescu, M. Liserre, and F. Blaabjerg, "Flexible active power control of distributed power generation systems during grid faults," *IEEE Trans. Ind. Electron.*, vol. 54, no. 5, pp. 2583–2592, Oct. 2007.
[35] A. Yazdani and R. Iravani, "A unified dynamic model and control for the voltage-sourced converter under unbalanced grid conditions," in *Proc. IEEE Power Eng. Soc. Gen. Meeting*, 2006, pp. 1–6.
[36] H.-S. Song and K. Nam, "Dual current control scheme for PWM converter under unbalanced input voltage conditions," *IEEE Trans. Ind. Electron.*, vol. 46, no. 5, pp. 953–959, Oct. 1999.
[37] P. Vas, *Electrical Machines and Drives, A Space-Vector Theory Approach*. Oxford, U.K.: Clarendon, 1992.
[38] X. Guo, W. Wu, and Z. Chen, "Multiple-complex coefficient-filter-based phase-locked loop and synchronization technique for three-phase grid-interfaced converters in distributed utility networks," *IEEE Trans. Ind. Electron.*, vol. 58, no. 4, pp. 1194–1204, Apr. 2011.
[39] K. Martin, "Complex signal processing is not complex," *IEEE Trans. Circuits Syst. I, Reg. Papers*, vol. 51, no. 9, pp. 1823–1836, Sep. 2004.
[40] IEEE Recommended Practice for Monitoring Electric Power Quality, IEEE Std. 1159-2009.
[41] J. Hu, Y. He, L. Xu, and B. Williams, "Improved control of DFIG systems during network unbalance using PI-R current regulators," *IEEE Trans. Ind. Electron.*, vol. 56, no. 2, pp. 439–451, Feb. 2009.
[42] M. Castilla, J. Miret, J. Matas, L. de Vicua, and J. Guerrero, "Linear current control scheme with series resonant harmonic compensator for single-phase grid-connected photovoltaic inverters," *IEEE Trans. Ind. Electron.*, vol. 55, no. 7, pp. 2724–2733, Jul. 2008.
[43] F. Rodriguez, E. Bueno, M. Aredes, L. Rolim, F. Neves, and M. Cavalcanti, "Discrete-time implementation of second order generalized integrators for grid converters," in *Proc. 34th IEEE IECON*, 2008, pp. 176–181.
[44] R. Vaccaro, *Digital Control: A State Space Approach*. New York: McGraw-Hill, 1995.
[45] S. Yang, Q. Lei, F. Peng, and Z. Qian, "A robust control scheme for grid-connected voltage-source inverters," *IEEE Trans. Ind. Electron.*, vol. 58, no. 1, pp. 202–212, Jan. 2011.

Claudio Alberto Busada was born in Bahía Blanca, Argentina, on March 13, 1962. He received the B.S. degree in electrical engineering and the Ph.D. degree in control systems from the Universidad Nacional del Sur (UNS), Bahía Blanca, in 1989 and 2004, respectively.

From 1988 to 2004, he was with the Mechanic and Electrical Department, City of Bahía Blanca. Since 1989, he has been with the Departamento de Ingeniería Eléctrica y de Computadoras, UNS, where he is a Professor. He is a Researcher with the Instituto de Investigaciones en Ingeniería Eléctrica "Alfredo C. Desages" [UNS–Consejo Nacional de Investigaciones Científicas y Técnicas (CONICET)]. His research interests are in power electronics, rotating machinery, active filters, automatic control, and integration of distributed energy systems.

Sebastián Gómez Jorge received the B.S. degree in electronics engineering and the M.S. degree from the Universidad Nacional del Sur (UNS), Bahía Blanca, Argentina, in 2006 and 2009, respectively, where he is currently working toward the Ph.D. degree in engineering.

He is currently with the Instituto de Investigaciones en Ingeniería Eléctrica "Alfredo Desages" [UNS–Consejo Nacional de Investigaciones Científicas y Técnicas (CONICET)], Departamento de Ingeniería Eléctrica y de Computadoras, UNS.

Andres E. Leon (S'05) was born in Argentina in 1979. He received the B.S. degree in electrical engineering from the Universidad Nacional del Comahue, Neuquén, Argentina, and the Ph.D. degree from the Universidad Nacional del Sur (UNS), Bahía Blanca, Argentina, in 2005 and 2011, respectively.

He is currently with the Instituto de Investigaciones en Ingeniería Eléctrica "Alfredo Desages" [UNS–Consejo Nacional de Investigaciones Científicas y Técnicas (CONICET)], Departamento de Ingeniería Eléctrica y de Computadoras, UNS. His primary areas of interest are power systems control, custom power systems, and wind energy conversion systems.

Jorge A. Solsona (SM'04) received the B.S. degree in electronics engineering and the Ph.D. degree from the Universidad Nacional de La Plata, La Plata, Argentina, in 1986 and 1995, respectively.

He is currently with the Instituto de Investigaciones en Ingeniería Eléctrica "Alfredo Desages" [Universidad Nacional del Sur (UNS)–Consejo Nacional de Investigaciones Científicas y Técnicas (CONICET)], Departamento de Ingeniería Eléctrica y de Computadoras, UNS, Bahía Blanca, Argentina, where he is involved in teaching and research on control theory and its applications to electromechanical systems.